Submission to *Geomorphology*

Channel initiation by surface and subsurface flows in a steep catchment of the Akaishi Mountains, Japan

Fumitoshi Imaizumi[a,*], Tsuyoshi Hattanji[b], and Yuichi S. Hayakawa[c]

[a] Graduate School of Life and Environmental Sciences, University of Tsukuba, Ikawa Experimental Forest, 1621-2, Ikawa, Aoi, Shizuoka, 428-0504, Japan

[b] Graduate School of Life and Environmental Sciences, University of Tsukuba, 1-1-1, Tennodai, Tsukuba, Ibaraki, 305-8577, Japan

[c] Center for Spatial information Science, University of Tokyo, 5-1-5 Kashiwanoha, Kashiwa-shi, Chiba, 277-8568, Japan

[*]corresponding author. Tel: +81-54-260-2419; Fax: +81-54-260-2626

E-mail address: imaizumi@sakura.cc.tsukuba.ac.jp (F. Imaizumi)

Abstract

Channel initiation, which is a key factor in the evolution of mountain landforms, is caused by a combination of various hydrogeomorphic processes. We modeled the channel initiation in steep mountains on the basis of the physical mechanism for sediment transport by surface and subsurface flows. Field investigations and Geographic Information Systems (GIS) analysis in the Higashi-gouchi catchment of central Japan showed that our model can well explain the area–slope relationship in steep and highly incised subcatchments, in which surface flow and shallow underground water would be the dominant flow components. In contrast, the area–slope relationship is not clear in gentler subcatchments, in which the contribution of deeper flow components (i.e., deep underground water) on the entire runoff is not negligible. Thus, the contribution of each runoff component to the total runoff is an important factor affecting the location of the channel head formed by surface and subsurface flows. Many channel heads in the deeply incised subcatchments in the Higashi-gouchi catchment have been formed by surface and subsurface flows, although many landslides have also occurred around the channel heads. Compared with the dominant flow components, activity of sediment supply from hillslopes might be a minor factor in determining the area–slope relationship for locating the channel head.

Key words: Channel heads, Area–slope relationship, Surface erosion, Landslide, GIS

1. Introduction

Channel initiation is a key factor in the evolution of mountain landforms. The hydrogeomorphic processes determining the location of the channel head vary from catchment to catchment. Montgomery and Dietrich (1988, 1989) proposed a physically based area–slope threshold of shallow landslides, which successfully explains the inverse area–slope relationship for the channel head location. In contrast, the inverse area-slope relationship for the channel head location can also be explained in terms of erosion by surface and subsurface flow in areas with less landslides (Dietrich et al., 1992; Hattanji et al., 2006; Hattanji and Matsushi, 2006). In either case, drainage area and slope gradient are important factors affecting the location of the channel head. Montgomery and Dietrich (1994) reported the area–slope relationships at channel heads under different lithologic and climatic conditions. In semiarid or Mediterranean environments, many researchers compared thresholds predicted by theoretical models with the observed area–slope relations at gully heads (Prosser and Abernethy, 1996; Vandaele et al., 1996; Vandekerckhove et al., 2000; Istanbulluoglu et al., 2002; Kirkby et al., 2003). The area–slope relationships determined by the previous studies are different because of the diversity of predominant hydrogeomorphic processes (i.e., sediment supply/transport processes and runoff components) that are affected by terrain, climate, soil depth, and geology (Montgomery and Dietrich, 1994; Vandekerckhove et al., 2000; Hattanji and Matsushi, 2006, McNamara et al., 2006).

Shallow landsliding is an often-recorded geomorphic process in humid forested mountains (Tsukamoto et al., 1973, 1982; Dietrich and Dunne, 1978; Iida and Okunishi, 1983; Dietrich et al., 1986). Almost all zero-order basins have shallow-landslide scars on some granitic hillslopes in Japan (Tsukamoto et al., 1973, 1982; Iida and Okunishi, 1983; Onda, 1992). Many prior studies on landslide dominant mountains have dealt with channel initiation caused by landslides (e.g., Dietrich et al., 1992; Montgomery and Dietrich, 1994). The contribution of other sediment supply and transport processes to channel initiation, however, has rarely been discussed.

Both dissected and gentle terrains exist in some mountainous regions in which the uplift rate is high (e.g., Sugai, 1990). In humid regions, landslides usually supply a large volume of sediment to steep terrain, whereas the frequency of landslides is lower and erosion by surface and subsurface flows is the predominant process in gentle terrain (e.g., Sidle and Ochiai, 2006; Imaizumi and Sidle, 2007). Thus, the frequency of landslides as well as the type of predominant runoff may vary between dissected and gentle areas. Dietrich et al. (1987) suggested that a channel head advances upstream by shallow landsliding and migrates downstream as a result of sediment supply from side slopes during the landslide recurrence interval. Thus, the area–slope relationship would not be constant in highly uplifting mountainous areas because of the wide range of local landslide frequencies. Moreover, other sediment supply processes (e.g., debris flow and dry ravels), which change the volume of the storage around channel (Imaizumi et al., 2006; Imaizumi and Sidle, 2007), possibly affect the channel head location.

The overall aim of this study is to examine the channel initiation based on physical modeling as well as field and Geographic Information Systems (GIS) investigations in the steep and rapidly uplifting Higashi-gouchi catchment in the Akaishi Mountains, central Japan. We studied the channel initiation caused by surface and subsurface flows in both deeply incised areas and relatively gentle areas of the catchment. Specific objectives included: (*i*) to make a physically based model that explains the channel initiation caused by entrainment of sediments by overland flow; (*ii*) to assess the area–slope relationship for the channel head location in mountainous catchments with a high uplifting rate by performing field surveys and an analysis using GIS and digital terrain models (DTM); and (*iii*) to clarify the influence of the predominant flow components as well as sediment supply activities on the area–slope relationship for the channel head location.

2. Physically based model

The channel-head location must be determined by a tradeoff between the frequency of shallow landsliding and the magnitude and frequency of bedload transport (Hattanji et al., 2006). In the limiting case with no landslides, the channel head locations would be controlled by the area–slope threshold for bedload transport (Dietrich et al., 1992, 1993; Montgomery and Dietrich, 1994; Hattanji et al., 2006). In mountains with frequent landslides, active sediment supply from lateral hillslopes possibly buries channels and facilitates downstream migration of channel heads. Furthermore, channel heads could advance upstream by shallow landsliding (Dietrich et al., 1987). By assuming that the channel head locations are completely determined by the area–slope threshold for the bedload transport, we propose a physical model for channel initiation by surface and subsurface flows (Fig. 1). The first step of the analysis for the modeling is to predict the shear stress for the sediment transport around the channel head:

$$\tau = \rho g R S \qquad (1)$$

where τ is the shear stress (N m^{-2}), ρ is the mass density of water (~1.0×10^3 kg m^{-3}), g is the acceleration of gravity (9.8 m s^{-2}) , R is the hydraulic radius (m), and S is the slope gradient. In Eq. (1), ρ and g are considered to be constant. Thus, we need to obtain the critical value of R for entrainment of sediment in the given topography S.

The second step of the analysis is to predict the peak hydraulic radius R at the channel head during heavy rainfall events. Many hydrologic studies have reported the discharge–rainfall intensity relationship at channel heads, especially during heavy rainstorm events (e.g., Montgomery et al., 1997; Uchida et al., 1999; Hattanji et al., 2006). In addition, previous models for channel initiation have assumed that the discharge increases in proportion to the drainage area (Dietrich et al., 1992, 1993; Montgomery and Dietrich, 1994; Hattanji et al., 2006). If the peak discharge Q_p (m^3 s^{-1}) resulting from a storm is directly proportional to the drainage area A (m^2) and the effective rainfall intensity I_R (m s^{-1}), then:

$$Q_p = k_p I_R A \qquad (2)$$

where k_p is a dimensionless coefficient equal to peak specific discharge per unit rainfall intensity (Hattanji et al., 2006). Peak discharge Q_p ($\mathrm{m^3\ s^{-1}}$) can be also estimated from the peak cross-sectional area at the channel head, a ($\mathrm{m^2}$), and the flow velocity v ($\mathrm{m\ s^{-1}}$) at that time:

$$Q_\mathrm{p} = av \qquad (3)$$

The flow velocity is given by Manning's equation, which appropriately estimates the flow velocity in open channels:

$$v = \mathrm{n}^{-1} R^{2/3} S^{1/2} \qquad (4)$$

where n is Manning's roughness coefficient. Note that Eq. (4) is for turbulent overland flow and is not applicable to laminar overland flow. By assuming that the cross-sectional area of the channel head is an inverted triangle (Fig. 1), R and a are determined by the water depth h as follows:

$$R = \mathrm{B}_1 h \qquad (5)$$

$$a = \mathrm{B}_2 h^2 \qquad (6)$$

where B_1 and B_2 are constants given by the cross-sectional gradient of the channel bed ϕ ($\mathrm{B}_1 = 2^{-1}\cos\phi$, $\mathrm{B}_2 = \tan\phi^{-1}$). By substituting Eqs. (3) and (6) into Eq. (2) and replacing h with R by using Eq. (5), the peak hydraulic radius is given as:

$$R = \left(\mathrm{B}_1{}^2 \mathrm{B}_2{}^{-1} \mathrm{n}\,\mathrm{k_p}\, I_\mathrm{R} A S^{-1/2}\right)^{3/8} \qquad (7)$$

The peak shear stress at the peak hydraulic radius is gotten by substituting Eq. (7) into Eq. (1):

$$\tau = \rho \mathrm{g} \left(\mathrm{B}_1{}^2 \mathrm{B}_2{}^{-1} \mathrm{n} \mathrm{k_p} I_\mathrm{R}\right)^{3/8} A^{3/8} S^{13/16} \qquad (8)$$

The channel head would advance upstream if the peak shear stress exceeds the critical shear stress τ_c of the sediment at the channel head. By equating τ and τ_c, the relationship between drainage area A and slope gradient S at the channel head is:

$$A = \mathrm{B} S^{-13/6} \qquad (9)$$

where B is a constant:

$$\mathrm{B} = \mathrm{B}_1{}^{-2} \mathrm{B}_2 \mathrm{n}^{-1} \mathrm{k_p}{}^{-1} I_\mathrm{R}{}^{-1} \left(\rho^{-1} \mathrm{g}^{-1} \tau_\mathrm{c}\right)^{8/3} \qquad (10)$$

Our model might not be able to account for the area–slope relationship if the location of the channel head were heavily affected by the sediment supply activity from hillslopes rather than the sediment transport condition given by Eq. (9). Upstream migration of the channel head caused by shallow landsliding might also obscure the area–slope relationship. In this study, we evaluated the influence of sediment supply and landsliding on the location of the channel head by comparing Eq. (9) with the actual slope–area relationship on site. Our model is partly based on the channel initiation model considering surface erosion by turbulent overland flow proposed by Dietrich et al. (1993). They assumed surface erosion on an inclined plane; the slope length (m) was used as a parameter for representing the drainage area in their model. In contrast, our model assumes water accumulation from a concave drainage area (with the dimension of m^2). Our model considers that water accumulates not only from surface flows, but also from subsurface flows that sometimes form channels through seepage erosion (e.g., McNamara et al., 2006), when the contributing area of the subsurface flow corresponds to that estimated by the topography. Note that our model does not consider upstream migration of the channel head caused by erosion of unchannelized regolith; higher stream power may be needed for the erosion of hillslope regolith because of its higher cohesion reinforced by roots.

3. Study area

We applied the physically based model to sedimentary rock mountains in the upper half of the drainage area of the Higashi-gouchi River (17.6 km^2), a tributary of the Ohi River, central Japan (Fig. 2). The Higashi-gouchi catchment is located in the Akaishi Mountains whose uplifting rate is the highest in Japan (4 mm yr^{-1}; Danbara, 1971). The lowest elevation in the Higashi-gouchi catchment is at the south end (900 m a.s.l.); the highest elevation is the peak of Mount Aonagi (2406 m a.s.l.) at the northwest end. The entire study area has been managed by the University of Tsukuba as the “Ikawa University Forest”; artificial forests of sugi (Japanese cedar, *Cryptomeria japonica*), hinoki (Japanese cypress, *Chamaecyparis* *obtusa*), and karamatsu (*Larix kaempferi*) occupy 17% of the catchment. Natural forest (77%; mainly secondary forest), landslides, and the riparian area occupy the rest of the catchment. A large part of the forest (mainly conifer trees) was harvested in the 1950s and 1960s. Other than forest management (replanting and thinning) in the artificial forests and construction of check dams along the Higashi-gouchi River, almost no anthropogenic disturbances have occurred since the harvest. The main geologic unit is the Shimanto Cretaceous strata comprised of sandstone and shale. Most of the catchment is characterized by very steep slopes; slopes with gradients of 35˚–45˚ comprise about 50% of the entire catchment. Brown forest soil covers most of the catchment.

The Higashi-gouchi catchment receives abundant rainfall (average 2800 mm annually in the period from 1993 to 2002). Heavy rainfall events (i.e., total rainfall > 100 mm) occur during the Baiu rainy season (June and July) and in the autumn typhoon season (late August to early October). Winter snowfall occurs from December to March, but precipitation in this period accounts for only about 15% of the total annual precipitation. Except the north-facing slopes, the annual maximum depth of snow cover is less than 20 cm; most of the snow melts within a week after a snowfall. Thus, snowmelt is typically not a significant sediment supply mechanism in this area. Landslides and debris flows associated with high precipitation during the Baiu rainy season and the typhoon season are the major sediment supply processes in this area (Maita et al., 1983; Matsushita et al., 2003). Investigations using color aerial photographs with a resolution of 40 cm taken in 2007 revealed that landslide area occupied 3.6% of the entire Higashi-gouchi catchment. Freeze-thaw that promotes dry ravel at landslide scars is also an important sediment supply process in this region (Maita, 1985; Imaizumi et al., 2006). The average erosion rate around the Higashi-gouchi catchment, as estimated from changes in the volume of deposits in the Ikawa Dam reservoir (13 km downstream of the catchment) from 1967 to 1991 divided by contributing area of the reservoir, is 7 mm yr^{-1}. The topography of the catchment is characterized by relatively gentler slopes around ridge lines, formed by periglacial processes (Sugai, 1990), and deeply incised valleys along the Higashi-gouchi River and its large tributaries.

Soil depth in gentler areas is thicker (0.5–2 m; Sugai, 1990) than in steeper areas (typically < 1 m).

4. Methodology

4.1. Analysis of catchment topography

The Ikawa University Forest conducted airborne LiDAR (Light Detection And Ranging; vertical accuracy, < 0.35 m) scanning on December 1, 2007, after fall of deciduous leaf and before snow cover. Interval of measure points by the scanning were 1.2 and 1.5 m for along-track and cross-track directions, respectively. The ground elevation points filtered by vegetations were interpolated into a 1-m resolution DTM using TIN model. This resolution of the DTM is considered to be sufficient to investigate channel head location as well as dominating sediment supply and transport processes (e.g., Tarolli and Fontana, 2009). Aerial photograph investigations conducted in the catchment showed that the landslide frequency was generally high in the terrain with high roughness, characterized by incised valleys and steep hillslopes (Matsushita et al., 2003). In contrast, the landslide frequency in the low roughness area was apparently lower than in the high roughness area (Matsushita et al., 2003). Thus, roughness of the terrain calculated from the DTM was used to classify subcatchments into two types: high roughness area (HRA) and low roughness area (LRA). We assumed that landslides and erosion by surface/subsurface flows were the predominant sediment supply process in HRAs and LRAs, respectively. Some prior studies proposed methods of determining surface roughness (e.g., McKean and Roering, 2004; Glenn et al., 2006). In this study, we used standard deviation of the slope gradient as a parameter of roughness, which successfully quantifies surface morphology (Frankel and Dolan, 2007). First, we visually separated the catchment into 43 subcatchments with similar catchment areas (average 0.4 km^2, Fig. 3). We set many subcatchment boundaries on low ridge lines which separate incised (high-roughness) and flat (low-roughness) tributaries. Second, the standard deviation of the slope gradient (tan θ) within a radius of 10 m was calculated for each

1-m grid cell using the 1-m resolution DTM (Fig. 4). We used tan θ, not degrees or radians, since the roughness calculated from tan θ has a larger weight in steeper terrains in which landslides usually occur. Finally, the average roughness was calculated for each subcatchment.

4.2. Field survey

We mapped the locations of sixteen channel heads by conducting field surveys. Exact locations of some channel heads were surveyed using a global positioning system (GPS; accuracy, 5–10 m) and a differential global positioning system (DGPS; accuracy, 2–3 m). We identified the channel heads based on the general definition of ‘‘the upstream boundary of concentrated water flow and sediment transport between definable banks’’ (Dietrich and Dunne, 1993). Exposure of bedrock and the formation of armor coats were evidence of sediment transport and surface water generation on site. Active sediment supply from hillslopes sometimes obscured banks and evidence of surface flow in some channels; these channels were also mapped and analyzed in this study. We classified the channel heads on the basis on their initiation mechanism; those formed by landslides (and subsequent debris flows) and those by surface/subsurface flow. Both surface erosion by overland flow and seepage erosion, which can be explained by our model, were treated together in this study.

We also measured the detailed topography around two channel heads on site (C1 and C2; Figs. 3 and 5). Topography around C1, which was characterized as steep hillslopes, incised valley, and thin regolith, agree with typical topographic characteristics in HRAs. On the contrary, as with typical topography in LRAs, topography around C2 was relatively gentle. We measured the cross-sectional topography along five cross-sectional lines around each channel head by using tape measures and a laser ranger. The distance between adjacent cross-sectional lines was about 40 cm, and the interval between each measuring point in individual cross-sectional lines was 5 cm. We also sampled sediments around the channel heads for grain size analysis (>2 kg at each site). The samples were dried in an oven at 110°C for 6 hours and then analyzed by using sieves with mesh sizes of 1, 2, 4, 8 and 16 mm. The diameter of the sediments >16 mm was manually measured by using a scale. Sediments of each grain size class were weighed with an electric balance. The topography and grain size distribution were used to evaluate the shear stress and critical shear stress at the channel head.

4.3. Analysis of channel heads by GIS

The topographic features around the sixteen channel heads, whose location was determined in the field surveys, were checked in the slope gradient distribution map drawn from the 1-m resolution DTM (Fig. 3). We could identify all of channel heads investigated in the field surveys on the slope distribution map. Distance between channel heads investigated using DGPS and those estimated from the slope gradient map was generally less than 10 m. This distance would be affected by accuracy of DGPS, resolution of the slope distribution map, and error associated with the detecting method for channel head locations on the slope map. We assumed that resolution of the slope gradient map was sufficient for locating channel heads with accuracy < 10 m. Since very steep topography in the Higashi-gouchi catchment prevents us from conducting field surveys at most of channel heads, we identified the location of the rest of the channel heads by using the slope gradient map. The channel gradients from the channel head to a point 10 m downstream (S in Fig. 1) were analyzed using the DTM. We investigated the channel gradient, not the slope gradient above channel heads, because our model is based on the sediment transport mechanism in channels. The catchment area above the channel heads (A in Fig. 1) was estimated from the flow direction of each cell, as calculated from the DTM (Jenson and Domingue, 1988).

5. Results

5.1. Classification of subcatchments

The frequency distribution of the average roughness in the catchment had two peaks around 0.17 and 0.23 (Fig. 6). Thus, we set the borderline between HRAs and LRAs at the average roughness of 0.20, at which there were clearly fewer catchments than in the lower and higher roughness classes. The HRAs classified by the GIS analysis were mainly located around the upper stream of the Higashi-gouchi River and along large tributaries, whereas the LRAs were mainly located near mountain ridge lines and areas far from large tributaries (Fig. 4). The ratio of landslide area to the entire area was 5.4% and 2.5% in the HRAs and LRAs, respectively. Average slope gradient in the HRAs (44˚) was higher than that in the LRAs (38˚). The ratio of gentle area (i.e., < 30˚) to the entire area was 7.5% and 19% in the HRAs and the LRAs, respectively, indicating that HRA terrain was apparently steeper than LRA terrain. Based on our classification, the channel head C1 was located in an HRA catchment, and C2 was in an LRA.

5.2. Channel head features

Grass cover on the channel heads was rarely found in the field surveys. The high crown density of trees and gravelly sediments around the channel heads might have prevented vegetation coverage. Thus, turbulent flow was considered to be a dominant flow type at the channel heads, rather than laminar overland flow that usually occurs on channels covered by grass (Montgomery and Dietrich, 1994). Some of the surface-flow channels were located downslope of old landslide scars. Landslide deposits fed by infilling processes (e.g., soil creep and dry ravel) were identified around these channel heads (e.g., C2 in Fig. 5). We could visually distinguish between channels initiated directly from landslides, which generally have wide channel heads (i.e., > 5 m), and those initiated from surface flow, which have narrow channel heads (< 5 m), by using the 1-m resolution DTM.

Cross-sectional profiles downstream of the channel head C1 showed clear banks on both sides of the channel, whereas the banks around C2 were not clear except at the exact location of the channel head (C2-3, Fig. 7). C2 was located downslope of an old and large landslide scar; deposits (depth < 1 m) composed of landslide sediment as well as in-filled sediment were found in the field survey (Figs. 5 and 7). The cross-sectional profiles around C1 and C2 had knickpoints in the slope gradient (Fig. 7). The relationship between the water depth and the hydraulic radius, estimated from the cross-sectional profile, varied around these knickpoints (Fig. 8). However, the overall relationship between water depth and hydraulic radius can be properly explained by the fitting line obtained by least squares regression analysis (Table 1). The constant B_1 for the best-fit line varied between C1 and C2 as well as amongst cross-sectional lines around the same channel head. The cross-sectional area of water flow increased sharply with increasing water depth (Fig. 8). A quadratic curve can well explain the relationship between the water depth and cross-sectional area (Table 1). Although coefficients of determination (R^2) and P value for the fitting curves of the water depth–area relationship generally exceeded those for the water depth–hydraulic radius relationship, the range of the constant B_2 was wider than that of B_1. The grains around the channel heads were relatively coarse; d_{50} around C1 and C2 was 40 and 50 mm, respectively (Fig. 9). Particles from 30 to 100 mm in diameter accounted for about 70% of the particles at C1 and C2.

5.3. Channel head locations

A total of 148 channel heads were identified in the field surveys and GIS analysis (Fig. 3). Of these, twenty-six were directly initiated from landslides and debris flow scars, much fewer than the ones formed by surface and subsurface flows (122 in total; 50 and 72 in the HRAs and LRAs, respectively). We did not analyze the location of channel heads formed by landslides and debris flows, and instead focused on the channel initiation caused by surface and subsurface flows. Many of the channel heads formed by the flows were located downslope of old landslide scars (78% and 62% in the HRAs and LRAs, respectively). Our GIS analysis revealed that many channel banks in the HRAs have unclear sections, whereas channel banks in the LRAs were relatively clear. Active sediment deposition on channels in the HRAs and/or more enhanced erosion of channel side walls in steeper terrain (Oguchi, 1997) likely obscured channel banks.

The GIS analysis did not reveal the exact location of some channel heads, especially in the HRAs, because of the complex topography around the channels. Hence, we did not analyze the locations of these channel heads.

The drainage area above a channel head was inversely related to the channel gradient in the log-log plots (Fig.10). The relationship was relatively clear in the HRAs. Best-fit curves for this relationship, which was expressed as Eq. (9) in theory, were obtained by the least squares method. The constant (B in Eq. (9)) and exponent for the HRAs were 4568 m^2 and -2.33, respectively. The coefficients of determination (R^2) for the best-fit power law relationship for the HRAs was 0.18 ($P < 0.01$). In contrast, the area–slope plots were widely scattered in the LRAs. The constant and exponent in the LRAs were 8340 m^2 and -0.62, respectively. R^2 for the best-fit power law relationship was 0.04 ($P = 0.19$). The slope gradient downstream of the channel head usually exceeded 0.5 in the HRAs, while the slope gradient of some channel heads in the LRAs were below 0.5 (Fig. 10). In addition, the drainage area above the channel head in the HRAs was usually from 2000 to 30000 m^2, whereas the drainage area in the LRAs was significantly larger (Fig. 10). Consequently, the channel heads in the LRAs could be characterized as having wider distributions of drainage area and slope gradient in comparison with those of the HRAs.

6. Discussion

6.1. Sediment transport at channel heads

The distribution of grain sizes around the two channel heads (C1 and C2) indicated that fine sediment was preferentially washed away by water (e.g., surface flow and seepage). Entrainment of fine particles during moderate rainfall events at the channel head was also observed in Japan (Terajima et al., 2001). Not only fine sediment but also coarser sediment is transported for formation of the channel head. Thus, transport conditions for coarse sediment left around channel heads should be discussed as part of the channel initiation process. The dimensionless shear stress, τ_* (Shields parameter), which is an index to compare shear stress values under different site conditions, is given by the following equation:

$$\tau^* = \tau\left[(\sigma-\rho)gd\right]^{-1} \qquad (11)$$

where σ is the mass density of the sediment (~2.65 kg m^{-3}), ρ is the mass density of water (~1.0 × 10^{3} kg m^{-3}), g is the acceleration of gravity (9.8 m s^{-2}), and d is the grain size of the sediment (m). Dimensionless critical shear stress τ_c^* is also given by Eq. (11) and replacing τ^* with τ_c^*. The dimensionless critical shear stress for entrainment of d_{50} sediment (τ_{c50}^*) usually ranges between 0.05 and 0.09 (Parker et al., 1982; Andrews, 1983; Ferguson, 1994) in gentler channels, while higher values of τ_{c50}^* (0.14–0.23) occur in some gravel-bed and boulder-bed rivers (Batalla and Martín-Vide, 2001; Lenzi et al., 2006; Imaizumi et al., 2009). In the case of $\tau_{c50}^* = 0.15$, the shear stress τ needed for entrainment of d_{50} sediment at sites C1 and C2 was 97 and 121 N m^{-2}, respectively. The hydraulic radius for these critical shear stresses calculated from Eq. (1) was 11 and 14 mm, respectively. Roughness of bedrock as well as reinforcement by organics (e.g., roots and woody debris) might increase the critical hydraulic radius for entrainment of sediments around channel heads (e.g., Gomi and Sidle, 2003). In any case, the water height for initiating the channel head may exceed 10 mm at the study site.

6.2. Locations of channel heads and topography types

The exponent of the area–slope relationship for the HRAs (-2.33) roughly corresponded to that of our physically based model (-13/6) using Eq. (9) (Fig. 10), indicating that our model can properly explain channel initiation in the HRAs. Since location of many channel heads were investigated only by DTM analysis, relationship between area–slope plots may be obscured by errors due to our detecting method for the channel head location (assumed maximum error, 10 m). Slope gradient that are highly affected by the local channel profile would be more sensitive to that error than the catchment area. The spatial variability of B_1 and B_2 (in Eqs. (5) and (6)) as well as that of the grain size, which directly affects critical shear stress for entrainment of sediment, might also have scattered area–slope plots. The topography of the bedrock-regolith boundary that controls the direction of the subsurface storm flow would approximate the surface topography in the case of shallow regolith (Hutchinson and Moore, 2000). Thus, shallow regolith in the HRAs might have resulted in a clear relationship between storm flow and drainage area, as needed for determining the theoretical area–slope relationship to be valid. In contrast, the slope–area relationship was not clear in the LRAs (Fig. 10). Because of its low landslide frequency and gentle terrain, the depth of the soil layer in the LRA (0.5–2 m) is generally deeper than in the HRA (< 1 m). In addition, as is obvious from the multiple ridges in the LRAs (e.g., area A in Fig. 3), highly fractured bedrock in the LRAs has slide surfaces in the deep layer. Therefore, groundwater in the LRAs likely infiltrates the deep layer through cracks. Hattanji and Matsushi (2006) showed that area–slope relationship was unclear in areas where deeper groundwater significantly contributes to the entire runoff. The difference in drainage area estimated from the surface topography and the actual drainage area might be a reason for the obscured area–slope relationship in the LRA.

In areas where infilling processes (i.e., soil creep, dry ravel) in and around landslide scars are active, channels initiated by landsliding may be easily buried by the infilling processes after original failure. Surface and subsurface flows would form new channel heads on these buried channels. Since width of landslide scars (generally > 10 m) is wider than channel heads formed by surface and subsurface flows (typically < 5 m), landslide scars are not continuously connected to the channels newly formed by surface and subsurface flows. Thus, even in the HRAs, number of channel head directly started from landslides and debris flow scars were much less than ones formed by surface and subsurface flows (11 and 50, respectively). Lin and Oguchi (2006) also reported the development of a drainage system within a large landslide scar near the Higashi-gouchi catchment.

The sediment supply rate in the HRAs would be much higher than in the LRAs because of high landslide frequency and steep slopes that promote dry ravel and rock fall. In fact, many channels in the

HRAs had sections that covered by sediments from hillslopes. However, the area–slope relationship in the HRAs was much clearer than in the LRAs (Fig. 10), indicating that sediment supply is a minor determining factor for the location of channel heads in comparison with the difference in the hydrological processes.

6.3. Comparison with other regions

A similar exponent in the area–slope relationship (Eq. (9)) has also been found in the Pacific Northwest, Belgium, Thailand, and Japan (Montgomery and Dietrich, 1994; Nachtergaele et al., 2001; Hattanji et al., 2006; McNamara et al., 2006), indicating that Eq. (9) is applicable to other humid regions. The exponent was higher than in semiarid areas, ranging from -2.4 to -9.6 (Vandekerckhove et al., 2000), although a higher exponent (≈ -0.5) was obtained from an analysis in which all of these semiarid data were plotted together (Kirkby et al., 2003). Prior studies have pointed out that difference in the dominating runoff components (i.e., surface flow, subsurface flow, and ground water) affects the variability of the exponent amongst catchments (Montgomery and Dietrich, 1994; Vandekerckhove et al., 2000). The difference in the flow type (i.e., turbulent and laminar flow) also affects it (Montgomery and Dietrich, 1994). The constant B in Eq. (9) for the Higashi-gouchi catchment was much larger than that of the other catchments reported in Hattanji and Matsushi (2006) (Table 2). The larger grain size in the Higashi-gouchi catchment might increase the critical shear stress and be the cause of the higher B. The difference in the contribution of ground water flow to the entire runoff also affects B (Hattanji and Matsushi, 2006). High relief energy in the Higashi-gouchi catchment may result in a large k_p value, which is inversely proportional to B (Eq. (10)). However, B was higher than in other catchments (Table 2), indicating that relief energy does not affect B as much as other factors. Locations of many channel heads in the Higashi-gouchi catchment were investigated only by DTM analysis. Hence, R^2 of the area–slope relationship in the Higashi-gouchi catchment would be lower than that in other regions (Table 2). Uniformity of the grain size and the cross-sectional profile of channel heads in individual study areas would also affect the R^2 of the area–slope relationship.

7. Conclusions

Channel initiation, which are key factors in the evolution of mountain landforms, were modeled on the basis of the physical mechanism for sediment transport by surface and subsurface flows. The peak discharge for sediment transport around channel heads was estimated by assuming that the discharge is proportional to the catchment area above the channel head. Physical analysis of sediment transport by surface and subsurface flows showed that the catchment area was inversely proportional to the channel gradient in the log-log plots; the exponent of the area–slope relationship in our model was equal to -13/6. Area–slope relationship in the Higashi-gouchi catchment of central Japan, as investigated by field surveys and GIS analysis, varied among the subcatchments. In the high roughness areas (HRAs) with high landslide frequency and highly incised topography, the area–slope relationship was clear, and the exponent of the fitting curves (= -2.33) was similar to that of our model (= -13/6). In contrast, the area–slope relationship was not clear in the low roughness areas (LRAs), in which landslides are infrequent. Shallow regolith in the HRAs might have resulted in a clear relationship between storm flow and drainage area, as needed for determining the theoretical area–slope relationship (Eq. (9)) to be valid. In the LRAs, deeper flow components would have obscured the drainage area–discharge relationship. Consequently, the type of runoff components would be the predominant factor affecting the area–slope relationship. Active sediment supply in the HRAs sometimes buries channel sections; however, the influence of the sediment supply on the area–slope relationship could not be ascertained.

Our study elucidated that many channels in the landslide dominating area, in which old landslide scars exist around most of the channel heads, were formed by surface and subsurface flows. Therefore, various hydrogeomorphic processes related to channel initiation should be considered to understand the evolution of mountain landforms. We also conclude that the difference in runoff components is the important factor affecting the location of channel heads, rather than the sediment supply rate. To demonstrate the influence of hydrological processes on channel initiation in detail, discharge observations as well as the detailed topographic surveys will have to be examined.

References

Andrews, E.D., 1983. Entrainment of gravel from naturally sorted riverbed material. Geological Society of America Bulletin 94, 1225–1231.

Batalla, R.J., Martín-Vide J.P., 2001. Thresholds of particle entrainment in a poorly sorted sandy gravel-bed river. Catena 44, 223–243.

Danbara, T., 1971. Synthetic vertical movements in Japan during the recent 70 years. Journal of the Geodetic Society of Japan 17, 100–108 (in Japanese with English abstract).

Dietrich, W.E., Dunne, T., 1978. Sediment budget for a small catchment in mountainous terrain, Z. Geomorphol. 29, suppl., 191–206.

Dietrich, W.E., Dunne, T., 1993. The channel head. In: Beven, K., Kirkby, M. J. (Eds), Channel Network Hydrology, John Wiley, Hoboken, N. J., pp. 175– 219.

Dietrich, W.E., Wilson, C.J., Reneau, S.L., 1986. Hollows, colluvium, and landslides in soil-mantled landscapes. In: Abrahams, A. D. (Eds.), Hillslope Processes, Allen and Unwin, Concord, Mass, pp. 361– 388.

Dietrich, W.E., Reneau, S.L., Wilson, C.J., 1987. Overview: ‘‘Zero order basins’’ and problems of drainage density, sediment transport and hillslope morphology. In: Beschta, R. L. et al. (Eds.), Erosion and Sedimentation in the Pacific Rim, IAHS Publ., vol. 165, Int. Assoc. of Hydrol. Sci., Wallingford, U. K, pp. 27–37.

Dietrich, W.E., Wilson, C.J., Montgomery, D.R., McKean, J., Bauer, R., 1992. Erosion thresholds and land surface morphology. Geology 20, 675– 679.

Dietrich, W.E., Wilson, C.J., Montgomery, D.R., McKean, J., 1993. Analysis of erosion thresholds, channel networks and landscape morphology using a digital terrain model. Journal of Geology 101, 259–278.

Ferguson, R.I., 1994. Critical discharge for entrainment of poorly sorted gravel. Earth Surface Processes and Landforms 19, 179–186.

Frankel, K.L., Dolan, J.F., 2007. Characterizing arid region alluvial fan surface roughness with airborne laser swath mapping digital topographic data. Journal of Geophysical Research 112, F02025.

Glenn, N.F., Streutker, D.R., Chadwick, D.J., Tahckray, G.D., Dorsch, S.J., 2006. Analysis of LIDAR-derived topography information for characterizing and differentiating landslide morphology and activity. Geomorphology 73, 131-148.

Gomi, T., Sidle, R.C., 2003. Bed load transport in managed steep gradient headwater streams of southeastern Alaska. Water Resources Research 39, 1336.

Hattanji, T., Matsushi, Y., 2006. Effect of runoff processes on channel initiation: comparison of four forested mountains in Japan. Transactions, Japanese Geomorphological Union 27, 319-336.

Hattanji, T., Onda, Y., Matsukura, Y., 2006. Thresholds for bed load transport and channel initiation in a chert area in Ashio Mountains, Japan: An empirical approach from hydrogeomorphic observations. Journal of Geophysical Research, 11, F02022.

Hutchinson, D.G., Moore, R.D., 2000. Throughflow variability on a forested hillslope underlain by compacted glacial till. Hydrological Processes 14, 1751– 1766.

Iida, T., Okunishi, K., 1983. Development of hillslopes due to landslides. *Z. Geomorphol.* 46, suppl., 67–77.

Imaizumi, F., Sidle R.C., 2007. Linkage of sediment supply and transport processes in Miyagawa Dam catchment, Japan. Journal of Geophysical Research 112, F03012.

Imaizumi, F., Sidle, R.C., Tsuchiya, S., Ohsaka, O., 2006. Hydrogeomorphic processes in a steep debris flow initiation zone. Geophysical Research Letters 33, L10404.

Imaizumi F., Gomi, T., Kobayashi, S., Negishi, JN, 2009. Changes in bedload transport rate associated with episodic sediment supply in a Japanese headwater channel. Catena 77, 207-215.

Istanbulluoglu, E., Tarboton, D.J., Pack, R.T., Luce, C., 2002. A probabilistic approach for channel initiation. Water Resources Research 38, 1325.

Jenson, S.K., Domingue, J.O., 1988. Extracting topographic structure from digital elevation data for geographic information system analysis. Photogrammetric Engineering and Remote Sensing 54, 1593-1600.

Kirkby, M.J., Bull, L.J., Poesen, J., Nachtergaele,j., Vandekerckhove, L. 2003. Observed and modelled distributions of channel and gully heads—With examples from SE Spain and Belgium. Catena 50, 415–434.

Lenzi, M.A., Mao, M., Comiti, F., 2006. When does bedload transport begin in steep boulder-bed streams? Hydrological Processes 20, 3517–3533.

Lin, Z., Oguchi, T., 2006. DEM analysis on longitudinal and transverse profiles of steep mountainous watersheds. Geomorphology 78, 77-89.

Maita, H., Ohtsubo, T., Kaijo, M. 1983. Measurements on the amount of regulated sediment in the natural channel of a torrential river. Transactions of the Japanese Forestry Society 94, 641-643 (in Japanese).

Maita, H. 1985. The movement and deposition of debris and the vegetation invasion on the landslide scars in the upper basin of the Oi River. Journal of the Japan society of Erosion Control Engineering, 38(1), 16-24 (in Japanese with English Abstract).

Matsushita, K., Amada, T., Miyamoto, K., Maita, H., Ohtsubo, T., 2003. Changes in spatial distribution of bare area in Higashigouchi catchment, tributary of Ohi River. Bulletin of Tsukuba University Forests 19, 61-75 (in Japanese).

Mckean, J., Roering, J., 2004. Objective landslide detection and surface morphology mapping using high-resolution airborne laser altimetry. Geomorphology 57, 331-351.

McNamara J.P., Ziegler A.D., Wood S.H., Vogler J.B., 2006. Channel head locations with respect to geomorphologic thresholds derived from a digital elevation model: A case study in northern Thailand. Forest Ecology and Management 224, 147–156.

Montgomery, D.R., Dietrich, W.E., 1988. Where do channels begin? Nature 336, 232– 234.

Montgomery, D.R., Dietrich, W.E., 1989. Source areas, drainage density, and channel initiation. Water Resources Research 25, 1907–1918.

Montgomery, D.R., Dietrich, W.E., 1994. Landscape dissection and drainage area–slope thresholds. In: Kirkby M. J. (Eds.), Process Models and Theoretical Geomorphology, John Wiley, Hoboken, N. J., pp. 221– 246.

Montgomery, D.R., Dietrich, W.E., Torres, R., Anderson, S.P., Heffner, J. T., Loague, K., 1997. Hydrologic response of a steep, unchanneled valley to natural and applied rainfall, Water Resources Research 33, 91–109.

Nachtergaele, J., Poesen, J., Steegen, A., Takken, I., Beuselinck, L., Vandekerckhove, L., Govers, G., 2001. The value of a physically based model versus an empirical approach in the prediction of ephemeral gully erosion for loess-derived soils. Geomorphology 40, 237– 252.

Oguchi, T., 1997. Drainage density and relative relief in humid steep mountains with frequent slope failure. Earth Surface Processes and Landforms 22, 107-120.

Onda, Y., 1992, Influence of water storage capacity in the regolith zone on hydrological characteristics, slope processes, and slope form. Z. Geomorphol. 36, 165–178.

Parker, G., Klingeman, P., McLean, D., 1982. Bedload and size distributions in paved gravel-bed streams. Journal of the Hydr. Division ASCE 108 HY4, 544–571.

Prosser, I.P., Abernethy, B., 1996. Predicting the topographic limits to a gully network using a digital terrain model and process thresholds. Water Resources Research 32, 2289–2298.

Sidle, R.C., Ochiai, H., 2006. Landslides: Processes, Prediction, and Land Use, Am. Geophys. Union Water Resour. Mono. 18, Am. Geophys. Union, Washington, DC, 312 p.

Sugai, T., 1990. The origin and geomorphic characteristics of the erosional low-relief surfaces in the Akaishi Mountains and the Southern part of the Mikawa Plateau, central Japan. Geographical Review of Japan 63A-12, 793-813 (in Japanese with English Abstract).

Tarolli, P., Dalla Fontana, G., 2009. Hillslope-to-valley transition morphology: new opportunities from high resolution DTMs. Geomorphology, printing.

Terajima, T., Sakamoto, T., Shirai, T., 2001. Bed load yield caused by subsurface water discharge in a forested 0-order basin in Hokkaido, Northern Japan. Transactions, Japanese Geomorphological Union 22, 1 – 22 (in Japanese with English abstract).

Tsukamoto, Y., Hiramatsu, S., Sinohara, S., 1973. Study on the growth of stream channel (III)—Relationship between 0 (zero) order channels and landslides. Journal of the Japan society of Erosion Control Engineering 26(2), 14– 20 (in Japanese).

Tsukamoto, Y., Ohta, T., Noguchi, H., 1982. Hydrological and geomorphological studies of debris slides on forested hillslopes in Japan. In: Walling, D. E., Recent Developments in the Explanation and Prediction of Erosion and Sediment Yield, IAHS Publ., vol. 137, Int. Assoc. of Hydrol. Sci., Wallingford, U. K., pp. 89–98.

Uchida, T., Kosugi, K., Mizuyama, T., 1999. Runoff characteristics of pipeflow and effects of pipeflow on rainfall-runoff phenomena in a mountainous watershed. Journal of Hydrology 222, 18-36.

Vandaele, K., Poesen, J., Govers, G., van Wesemael, B., 1996. Geomorphic threshold conditions for ephemeral gully incision. Geomorphology 16, 161–173.

Vandekerckhove, L., Poesen, J., Wijdenes, D.O., Nachtergaele, J., Kosmas, C., Roxo, M.J., de Figueiredo, T., 2000. Thresholds for gully initiation and sedimentation in Mediterranean Europe. Earth Surface

Processes and Landforms 25, 1201– 1220.

Figure legends

Fig. 1. Schematic diagram showing the location and topography of a channel head. (a) Catchment area and slope gradient of a channel head. (b) Cross-sectional topography of the channel head.

Fig. 2. Map of Higashi-gouchi catchment.

Fig. 3. Slope gradient map of the Higashi-gouchi catchment. The location of the channel head is also shown. Detailed topography around C1 and C2 was measured on site. Multiple ridges exist in area A. The photo is a channel head initiated by landsliding; the black arrow shows its location.

Fig. 4. Spatial distribution of roughness and subcatchment type. (a) Spatial distribution of roughness. (b) Type of subcatchment classified using average roughness in individual subcatchments. Locations of the channel heads are also shown.

Fig. 5. Topography and view around channel heads C1 and C2. (a) Distribution of slope gradient around C1 and C2. Arrows point out the locations of the channel heads, and their direction shows the direction of photographs in (b). The white dashed line upstream of C2 indicates an old landslide scar, and the red dashed line surrounds landslide deposits. (b) Photographs taken around C1 and C2. The dashed lines show the outline of the channel heads. Yellow and white tapes in the photograph of C2 indicate the directions of longitudinal and transverse sections of the channel, respectively.

Fig. 6. Histogram of the average roughness in individual subcatchments.

Fig. 7. Topography around channel heads. (a) Cross-sectional profiles of channel heads C1 and C2. (b) Longitudinal profile along the dashed line in (a).

Fig. 8. Hydraulic radius (a) and cross-sectional area (b) versus water depth along five cross-sectional lines at channel heads C1 and C2.

Fig. 9. Grain size distribution at channel heads C1 and C2

Fig. 10. Plot of slope gradient (tan θ) and drainage area above a channel head. Channel heads initiated directly from landslides are not plotted.

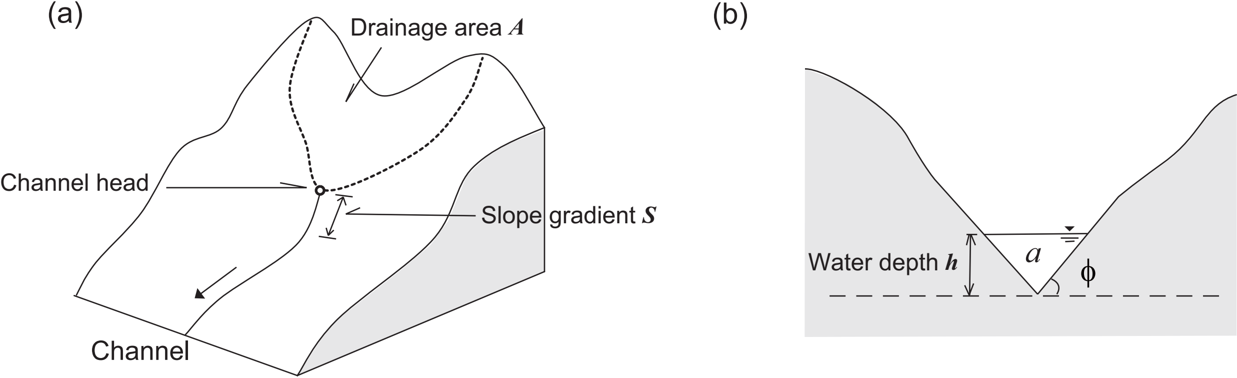
(a)
Drainage area A
Channel head
Slope gradient S
Channel
(b)
Water depth h
a
ϕ

Figure 1

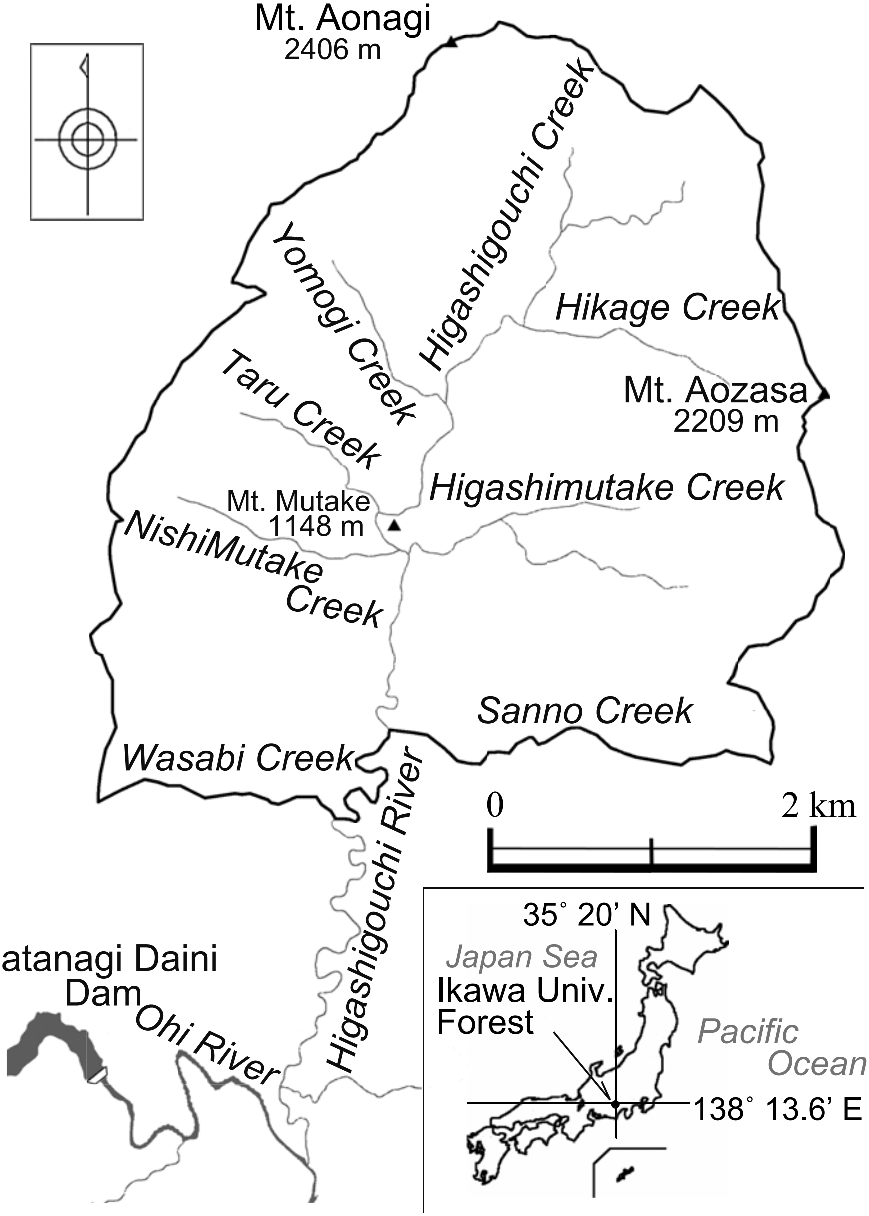
Mt. Aonagi
2406 m
Higashigouchi Creek
Yomogi Creek
Hikage Creek
Taru Creek
Mt. Aozasa
2209 m
Higashimutake Creek
Mt. Mutake
1148 m
NishiMutake
Creek
Sanno Creek
Wasabi Creek
Higashigouchi River
0
2 km
35° 20' N
Japan Sea
Ikawa Univ.
Forest
Pacific
Ocean
138° 13.6' E
Hatanagi Daini
Dam
Ohi River

Figure 2

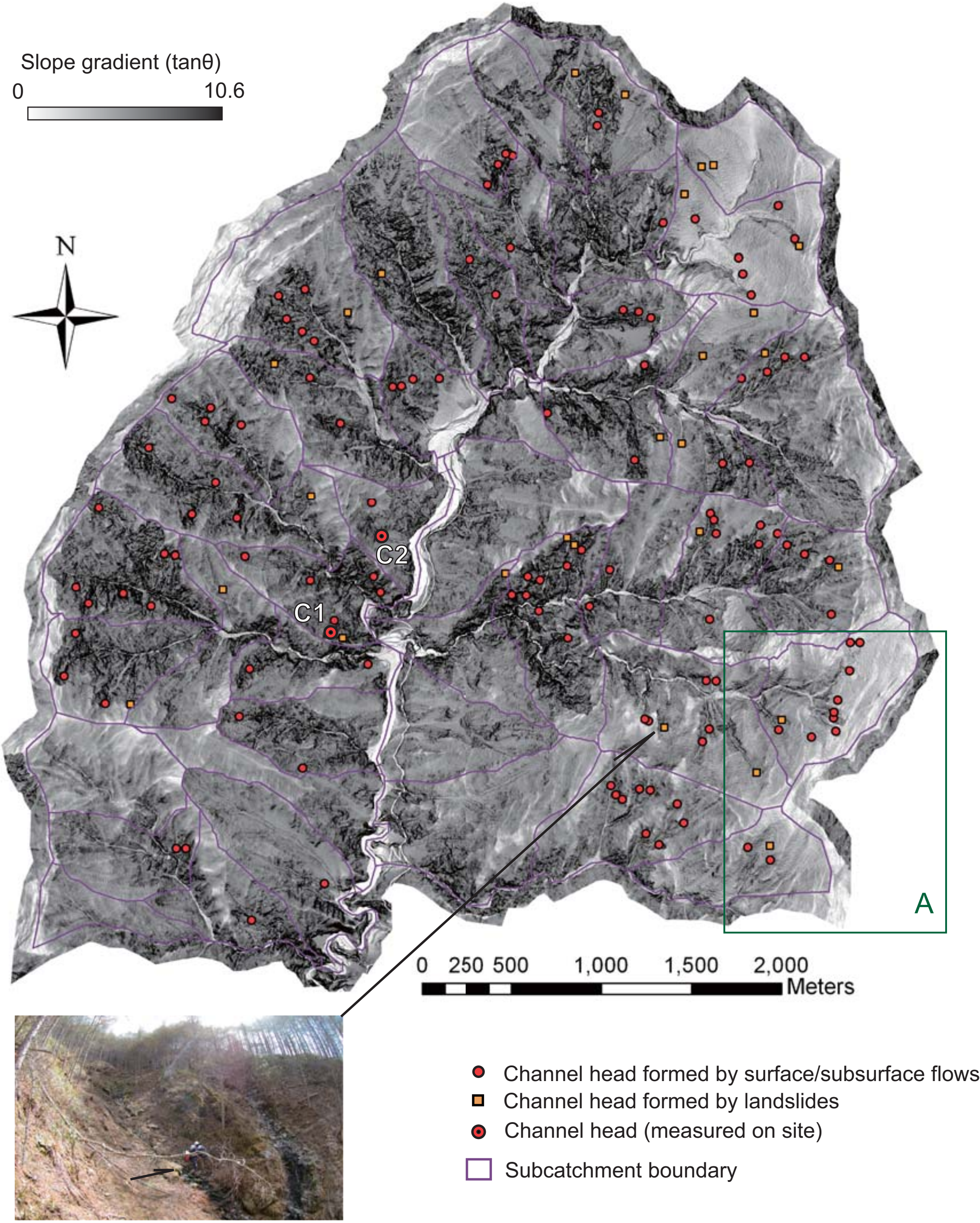

Slope gradient (tanθ)
0
10.6
N
C2
C1
A
0 250 500 1,000 1,500 2,000
Meters
Channel head formed by surface/subsurface flows
Channel head formed by landslides
Channel head (measured on site)
Subcatchment boundary

Figure 3

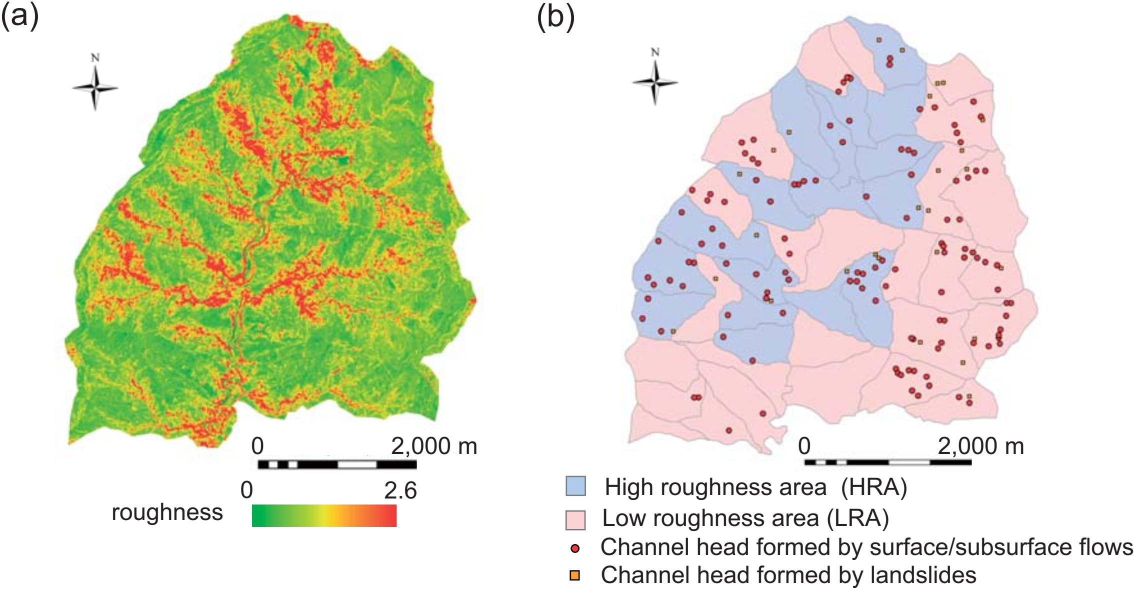
(a)
N
0
2,000 m
0
2.6
roughness
(b)
N
0
2,000 m
High roughness area (HRA)
Low roughness area (LRA)
Channel head formed by surface/subsurface flows
Channel head formed by landslides

Figure 4

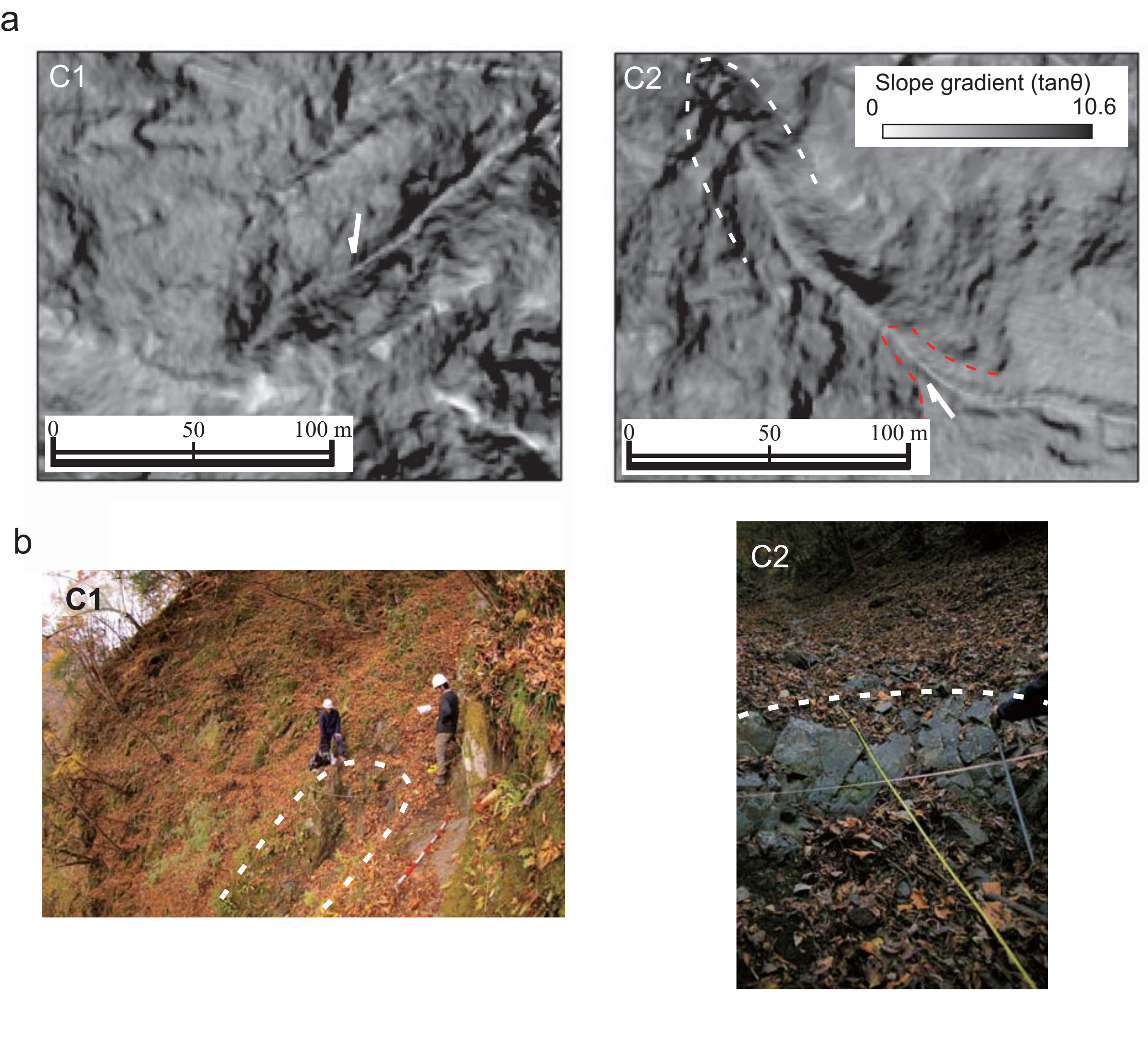

Figure 5

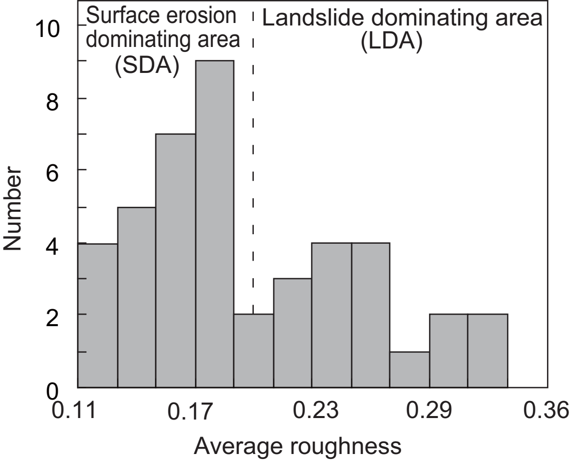
Surface erosion dominating area (SDA)
Landslide dominating area (LDA)
Number
0
2
4
6
8
10
0.11
0.17
0.23
0.29
0.36
Average roughness

Figure 6

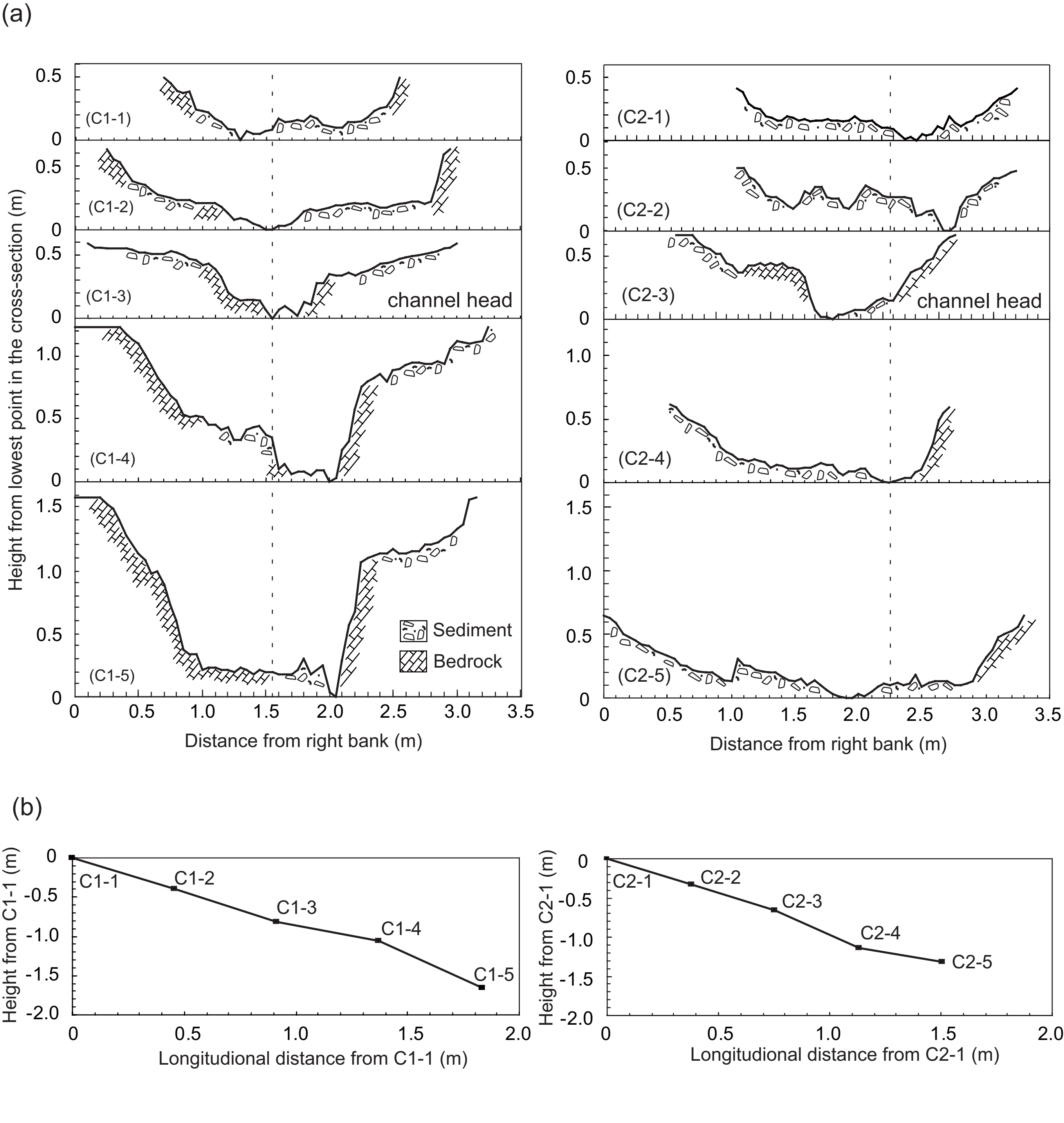
(a)
Height from lowest point in the cross-section (m)
(C1-1)
(C1-2)
(C1-3)
channel head
(C1-4)
(C1-5)
Sediment
Bedrock
Distance from right bank (m)
(C2-1)
(C2-2)
(C2-3)
channel head
(C2-4)
(C2-5)
Distance from right bank (m)
(b)
Height from C1-1 (m)
C1-1
C1-2
C1-3
C1-4
C1-5
Longitudional distance from C1-1 (m)
Height from C2-1 (m)
C2-1
C2-2
C2-3
C2-4
C2-5
Longitudional distance from C2-1 (m)

Figure 7

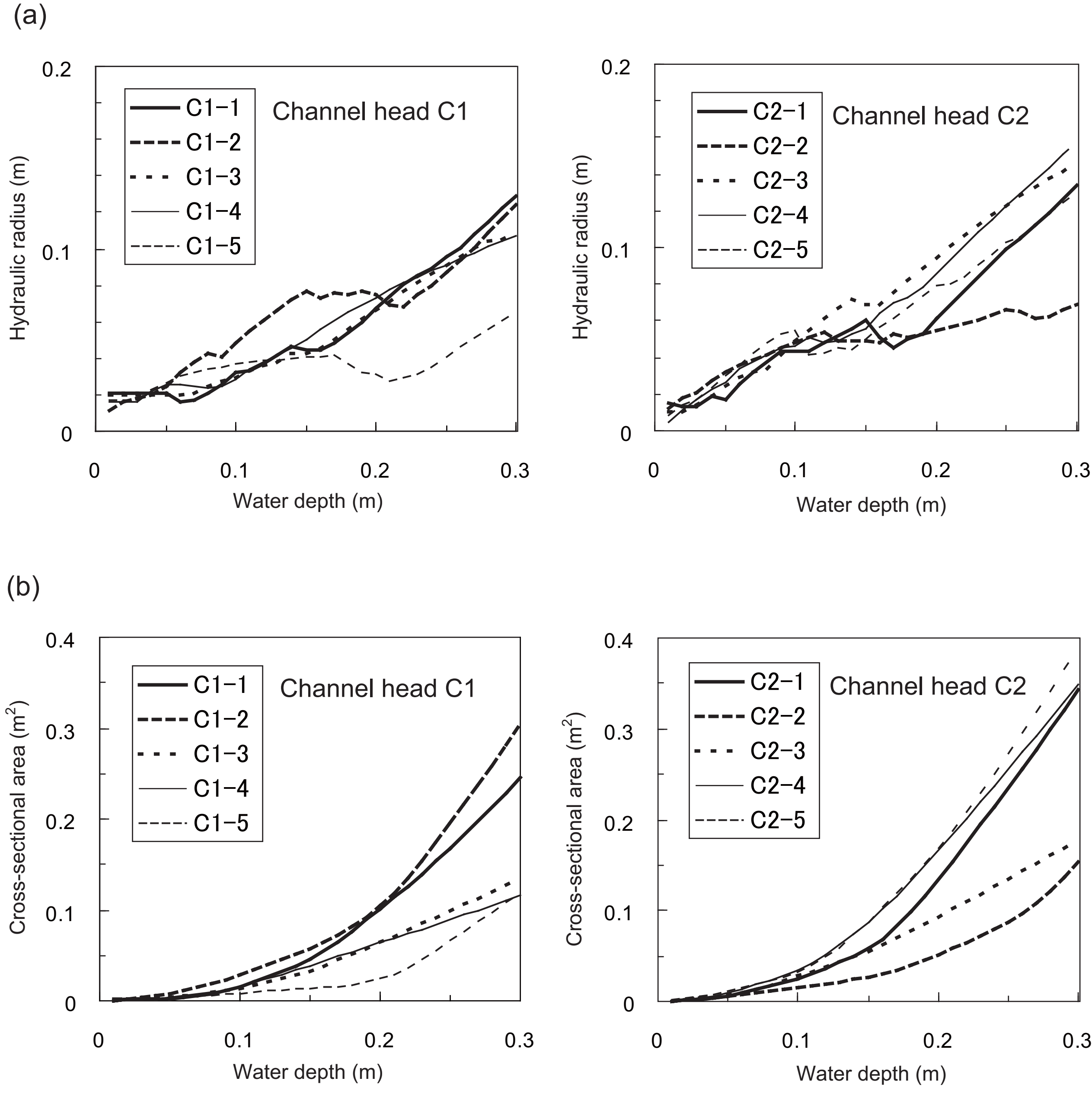
(a)
Channel head C1
C1−1
C1−2
C1−3
C1−4
C1−5
Hydraulic radius (m)
Water depth (m)
0
0.1
0.2
0.3
Channel head C2
C2−1
C2−2
C2−3
C2−4
C2−5
(b)
Cross-sectional area (m2)
0.4

Figure 8

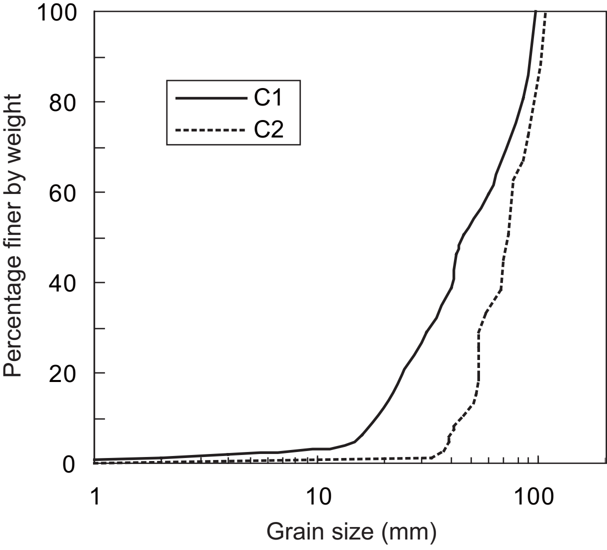
100
80
60
40
20
0
Percentage finer by weight
C1
C2
1
10
100
Grain size (mm)

Figure 9

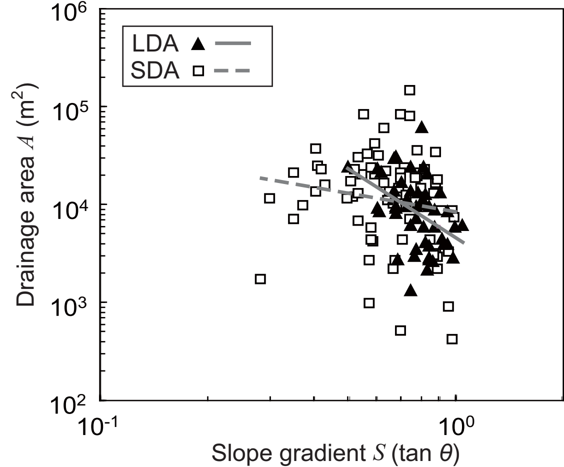

LDA
SDA
10^6
10^5
10^4
10^3
10^2
Drainage area A (m^2)
10^{-1}
10^0
Slope gradient S (tan θ)

Figure 10

Table 1. Coefficients and correlations for the relationships between water depth and hydraulic radius, and between water depth and cross-sectional area. (a) B_1 of the best-fit lines for the relationship between water depth and hydraulic radius (Eq. 5). (b) B_2 of the best-fit curves for the relationship between water depth and cross-sectional area of flow (Eq. 6). The coefficient of determination and the P value for each fitting equation are also listed.

(a)

line	B_1	R^2	P
C1-1	0.369	0.980	<0.01
C1-2	0.393	0.978	<0.01
C1-3	0.347	0.988	<0.01
C1-4	0.359	0.994	<0.01
C1-5	0.203	0.893	<0.01
C2-1	0.385	0.980	<0.01
C2-2	0.277	0.935	<0.01
C2-3	0.483	0.999	<0.01
C2-4	0.473	0.990	<0.01
C2-5	0.407	0.987	<0.01

(b)

line	B_2	R^2	P
C1-1	2.64	0.995	<0.01
C1-2	3.12	0.992	<0.01
C1-3	1.55	0.999	<0.01
C1-4	1.42	0.993	<0.01
C1-5	1.06	0.945	<0.01
C2-1	3.66	0.993	<0.01
C2-2	1.48	0.989	<0.01
C2-3	2.14	0.995	<0.01
C2-4	4.01	0.999	<0.01
C2-5	4.30	0.999	<0.01

Table 2 Area-slope relationship at the channel head in several regions in Japan, as determined by Eq. (9).

Area	Rock type	B	exponent	R^2
Ashio [a]	chert	750	-2.5	0.56
Ashio [a]	sandstone	580	-2.1	0.37
Kanozan [a]	mudstone	170	-2.0	0.43
Higashi-gouchi [b]	sandstone and shale	4568	-2.3	0.18

[a] Hattanji and Matsushi (2006), [b] High roughness areas (HRAs) in this study